Transport properties and electronic phase diagram of single-crystalline $Ca_{10}(Pt_3As_8)((Fe_{1-x}Pt_x)_2As_2)_5$

Z. J. Xiang, X. G. Luo, J. J. Ying, X. F. Wang, Y. J. Yan, A. F. Wang, P. Cheng, G. J. Ye, and X. H. Chen*

Hefei National Laboratory for Physical Science at Microscale and Department of Physics, University of Science and Technology of China, Hefei, Anhui 230026, People's Republic of China

(Received 8 March 2012; revised manuscript received 13 May 2012; published 22 June 2012)

Sizable single-crystalline samples of $Ca_{10}(Pt_3As_8)((Fe_{1-x}Pt_x)_2As_2)_5$ (the 10-3-8 phase) with $0 \leqslant x < 0.1$ have been grown and have been systematically characterized via x-ray diffraction, magnetic, and transport measurements. The unsubstituted sample is a heavily doped semiconductor with no sign of magnetic order down to 2 K. With increasing Pt content, the metallic behavior appears, and superconductivity is realized for $x \geqslant 0.023$. T_c rises to its maximum of approximately 13.6 K at the doping level of $x \sim 0.06$ and then decreases for higher x values. The electronic phase diagram of the 10-3-8 phase was mapped out based on the magnetic and transport measurements. The mass anisotropy parameter $\Gamma \sim 10$, obtained from resistive measurements in magnetic fields, indicates a relatively large anisotropy in the iron-based superconductor family. This strong two-dimensional character may lead to the absence of magnetic order. A linear T dependence of susceptibility at high temperatures is observed, indicating that spin fluctuations exist in the underdoped region as in most of the Fe-pnictide superconductors.

DOI: 10.1103/PhysRevB.85.224527 PACS number(s): 74.25.Ha, 74.25.F−, 74.25.Dw

I. INTRODUCTION

In the discovered high-temperature superconductors (SCs), which include cuprates and iron-based superconductors, superconductivity is often found in proximity to a magnetically ordered state. The parent compounds of cuprates are antiferromagnetic (AFM) insulators, whereas, for iron-based superconductors, the parent compounds are antiferromagnetic "semimetals." By charge injection via chemical substitution, magnetic order is suppressed, and superconductivity appears in both of these two families. Today, it is widely accepted that there is an intimate connection between magnetism and superconductivity in the high-temperature superconductors. Different from the cuprates in which Mott physics is dominant and the magnetic order is a Heisenberg AFM order of localized spins, the magnetic order of the Fe pnictides is mainly regarded as spin-density wave (SDW) type and exhibits a significant itinerant character. Most of Fe-pnictide superconductors have an antiferromagnetic region next to or overlapping with the superconducting region in their electronic phase diagrams.[1–5] Many theories suggest that the spin dynamics play a crucial role in the pairing mechanism for the superconductivity in the Fe-pnictide superconductors,[6,7] and it is conjectured that AFM spin fluctuations mediate the $s_{\pm}$ pairing and are responsible for the high T_c in Fe pnictides.[8–10] However, there are several kinds of Fe-pnictide superconductors for which a long-range magnetic order has not been reported, such as LiFeAs (Ref. 11) and so-called "perov-FeAs" materials. The latter is a group of layered materials in which FeAs layers are separated by perovskite-type layers. The chemical formula of perov-FeAs is either $(A_{n+1}M_nO_{3n-1-y})(Fe_2P_2)$ or $(A_{n+2}M_nO_{3n-y})(Fe_2P_2)$, where Ae represents alkaline-earth elements, M stands for metallic elements, and Pn represents pnictogens with A = Ca, Sr, Ba and M = Mg, Al, Sc, Ti, V, Cr, Co, etc.,[12–16] among which, the highest T_c ever reported is ∼47 K for $(Ca_4(Mg,Ti)_3O_y)(Fe_2As_2)$.[17] All of these nonmagnetic Fe-pnictide materials are intrinsic superconductors that show superconductivity in the stoichiometric compound. Recently, a new type of layered Fe-pnictide superconductor, $Ca_{10}(Pt_3As_8)((Fe_{1-x}Pt_x)_2As_2)_5$ (the 10-n-8 phase, n = 3,4) was discovered.[18–20] These materials have complex crystal structures with triclinic symmetry (space group P-1) in which Fe_2As_2 layers alternate with Pt_nAs_8 layers forming a -Ca-(Pt_nAs_8)-Ca-(Fe_2As_2)- stacking. We noticed that, for the 10-3-8 phase, the stoichiometric compound $Ca_{10}(Pt_3As_8)(Fe_2As_2)_5$ is nonsuperconducting and shows no visible magnetic transitions, whereas, electron doping through partial replacing Fe by Pt in the Fe_2As_2 layers induces superconductivity. These characters are special in the family of Fe-pnictide superconductors. In this paper, we report the results of a systematic study of the transport and magnetic properties of single-crystalline $Ca_{10}(Pt_3As_8)((Fe_{1-x}Pt_x)_2As_2)_5$ in different doping regions and present a corresponding electronic phase diagram. All the data indicated that there is no magnetic order in this system. The undoped sample is a semiconductor instead of an AFM semimetal. Superconductivity emerges upon 5d transition-metal Pt substituting on the Fe site as in the case of Pt-doped 122-type Fe-pnictide superconductors.[21,22] T_c reaches its maximum ∼13.6 K at the doping level $x \sim 0.06$, and further doping slowly suppresses T_c. The overdoped samples gradually exhibit a phase separation so that the SC region is not a perfect dome-shaped one. We also mentioned that the AFM spin fluctuations still exist in this system as well as in other Fe-pnictide superconductors, and the reason for the absence of AFM order might be ascribed to the high anisotropy of the 10-3-8 phase.

II. SAMPLE GROWTH AND CHARACTERIZATION

Single crystals of the 10-3-8 phase were grown by the self-flux method. Precursors CaAs and FeAs were prepared by reacting the mixture of the elements in the evacuated quartz tubes at 923 K for 24 h and at 973 K for 12 h, respectively. The starting materials CaAs, FeAs, and Pt were mixed by a ratio of $2{:}2{:}(0.6+x)$ (x = 0,0.1,0.2,0.3,0.4) in an argon-filled glove

box, thoroughly ground and set into alumina crucibles. The crucibles were sealed in evacuated quartz tubes and then were heated to a temperature above 1273 K at a rate of 100 K/h. For the superconducting samples, the best reaction temperature is 1323 K. The tubes were kept at this temperature for 75 h and then were cooled to 1173 K at a rate of 4.5 K/h. Finally, the quartz tubes were cooled in the furnace after shutting off the power. For the undoped compound, we chose a higher reaction temperature of 1423 K, and the reaction time was prolonged to 100 h, whereas, the starting ratio of CaAs, FeAs, and Pt was fixed at 2:2:1.05. After cooling, we obtained several dark-gray granules with typical dimensions of $4 \times 4 \times 3$ mm^3 together with a small amount of gray powder in each crucible. The shining platelike 10-3-8 crystals were cleaved from the internal parts of the granules. Single crystals were characterized by x-ray diffraction (XRD) using Cu K_α radiation. The actual chemical composition of the single crystals was determined by energy dispersive x-ray spectroscopy (EDS). The in-plane electrical transport was measured with the Physical Property Measurement System (Quantum Design, Inc.) using the ac four-probe method. The Hall effect was measured by the four-terminal ac technique. Magnetic susceptibility of the superconducting state was measured using a Quantum Design, Inc. superconducting quantum-interference device magnetometer. Normal-state susceptibility was measured by a vibrating sample magnetometer.

III. RESULTS AND DISCUSSIONS

The typical size of cleaved single crystals is about $2 \times 3 \times 0.1$ mm^3 as shown in Fig. 1(a). Figure 1(b) shows the single-crystal XRD patterns. Only (00l) reflections are observed, indicating that the single crystals are in perfect (001) orientation. The FWHM in the rocking curve of the (004) peak is 0.09°–0.20°, which indicates the single crystals are of high quality. Determined by the results of EDS, the atomic ratios of the single crystals that are cleaved from different granules in the same batch are slightly different, but the chemical composition is approximately uniform within one granule. The EDS results of samples from different starting material ratios are shown in Table I. The Pt-doping concentrations in the Fe_2As_2 layer were calculated from the relative atom ratio

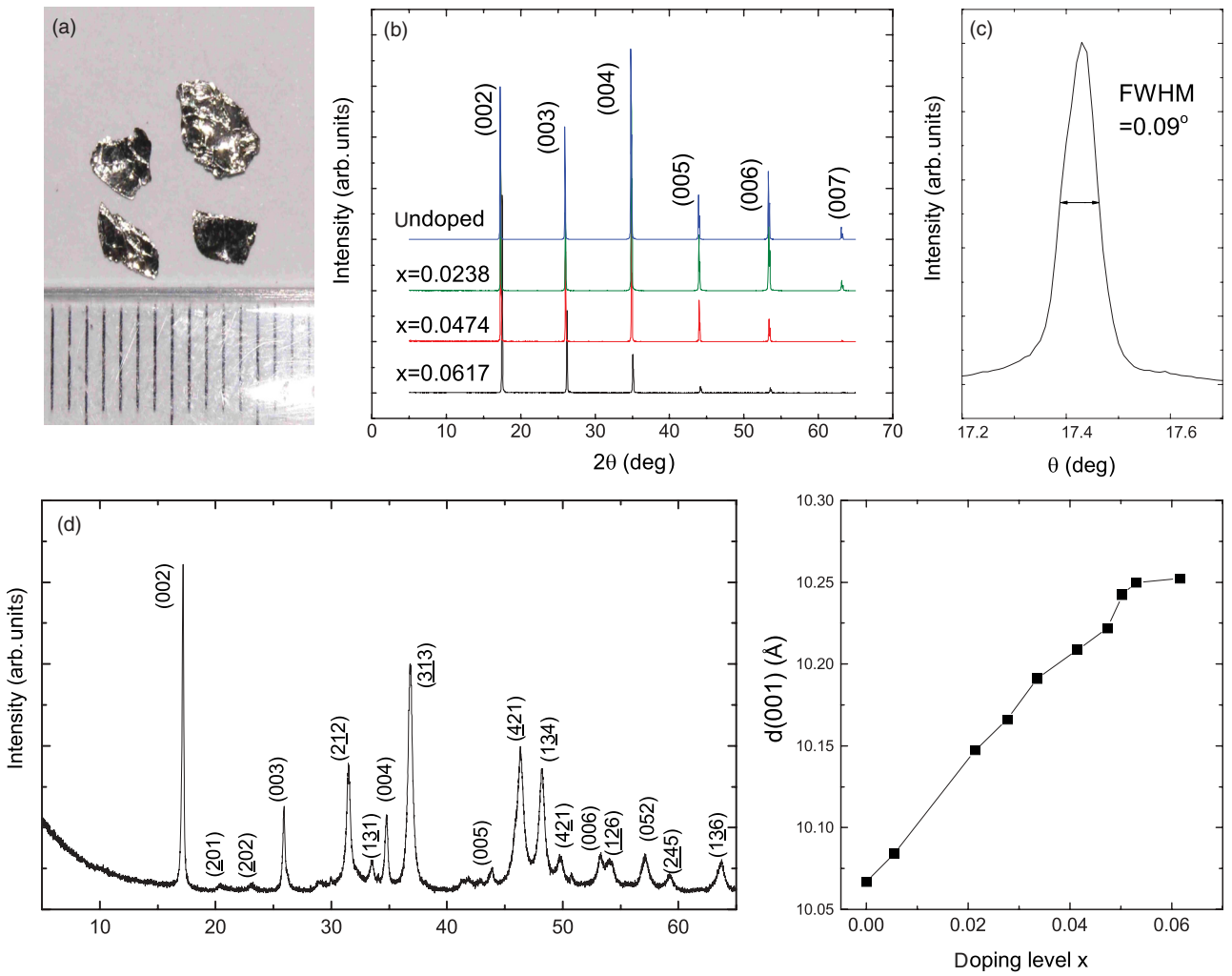

FIG. 1. (Color online) (a) Photograph of single-crystal pieces of $Ca_{10}(Pt_3As_8)((Fe_{1-x}Pt_x)_2As_2)_5$. (b) X-ray diffraction pattern of single crystals. (c) Rocking curve of the (004) reflection with the full width at half maximum (FWHM). (d) X-ray powder diffraction pattern of an underdoped sample with doping level $x \approx 0.025$. (e) Doping dependence of the interlayer spacing of the Fe plane.

TABLE I. Atom ratios in the 10-3-8 phase.

Sample number	Starting ratio Ca:Fe:Pt:As	EDS results Ca:Fe:Pt:As	Doping level x
1	2:2:1.05:4	2:2.083:0.598:3.558	Undoped
2	2:2:0.6:4	2:1.958:0.643:3.577	0.0213
3		2:1.960:0.675:3.527	0.0238
4		2:1.932:0.667:3.510	0.0335
5	2:2:0.7:4	2:1.946:0.682:3.540	0.0375
6		2:1.926:0.686:3.548	0.0415
7		2:1.957:0.707:3.560	0.0449
8	2:2:0.8:4	2:1.909:0.696:3.494	0.0474
9		2:1.942:0.716:3.499	0.0502
10	2:2:0.9:4	2:1.908:0.711:3.540	0.0530
11		2:1.888:0.727:3.550	0.0617
12	2:2:1.0:4	2:1.858:0.820:3.558	0.0981

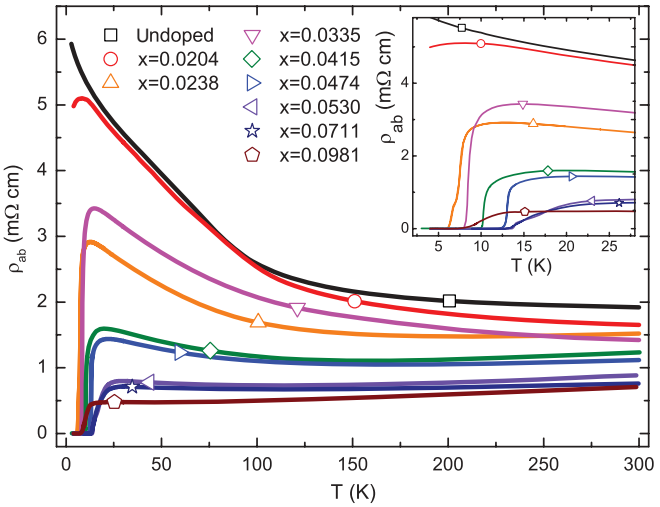

FIG. 2. (Color online) The temperature dependence of resistivity for $Ca_{10}(Pt_3As_8)((Fe_{1-x}Pt_x)_2As_2)_5$ samples. The inset shows an expanded plot.

of iron and platinum by assuming that there was neither Pt vacancy nor Fe substitution in the Pt_3As_8 layer according to the structure analysis in previous papers.[18–20] When doping concentration was $x > 0.075$, it became rather difficult to get the pure 10-3-8 phase. The XRD pattern of single crystals in the overdoped region usually shows two sets of (00l) diffraction peaks where one corresponds to the 10-3-8 phase and the other has larger (001) spacing (more than 10.3 Å), which can be attributed to the existence of the so-called "10-4-8" phase[18,19] intergrowing with the 10-3-8 phase. Sample No. 12 in Table I with $x = 0.0981$, which is discussed in this paper as the overdoped sample, does not show the intergrowing phenomenon. We did not succeed in growing the single phase sample with doping level $x > 0.1$.

Figure 1(d) shows the powder XRD pattern of the underdoped 10-3-8 phase. The powder was obtained by grinding single-crystal pieces, and the Miller indices were marked according to a triclinic (P-1) unit-cell symmetry. The lattice parameters determined by powder diffraction were estimated to be $a = 8.7608$, $b = 8.7551$, $c = 10.6831$ Å; $\alpha = 94.6823°$, $\beta = 104.2267°$, $\gamma = 89.9874°$. These values are generally in accordance with former results.[18] Figure 1(e) presents the evolution trend of the interlayer distance of two neighboring Fe-Fe square planes with Pt doping into FeAs layers. The interlayer distance [$d(001)$] increases rapidly in the underdoped region, whereas, the variation slows down when approaching optimal doping. As for $x > 0.05$, the value of $d(001)$ is almost unchanged with Pt content.

Figure 2 shows the temperature dependence of in-plane resistivity of $Ca_{10}(Pt_3As_8)((Fe_{1-x}Pt_x)_2As_2)_5$ single crystals. The behavior of resistivity of the undoped sample $Ca_{10}(Pt_3As_8)(Fe_2As_2)_5$ is obviously different from those of the undoped compound of the other iron-based superconductors. The parent compounds of 1111 and 122 Fe-based superconductors are so-called semimetals, and an abnormal feature in resistivity is observed at the antiferromagnetic transition/structural transition.[23,24] In this case, the unsubstituted sample is a heavily doped semiconductor, and the resistivity increases with cooling in the entire temperature range from 300 to 2 K. Below about 100 K, a sharp increase in $-d\rho/dT$ was observed, but no magnetic anomaly was seen down to 2 K. The value of resistivity at room temperature is on the same order of magnitude with polycrystalline LaFeAsO,[25] 1 order of magnitude larger than the $BaFe_2As_2$ single crystal and 1 and 2 orders of magnitude smaller than the nonsuperconducting $(Sr_4Sc_2O_6)(Fe_2As_2)$ (Ref. 26) and the semiconducting phase of $K_xFe_{2-y}Se_2$,[27] respectively. With Pt doping into the Fe_2As_2 layers, the resistivity gradually decreases, and metallic behavior emerges at high temperatures. For samples with $0.015 < x < 0.023$, the resistivity still shows a semiconducting behavior but decreases below about 8 K without reaching zero, which can be regarded as a trace of superconductivity. With further Pt doping, zero resistivity was observed. The zero resistivity temperature $T_c(0)$ can reach the maximum of 13.6 K in the samples with $x = 0.0530$ and $x = 0.0617$ and decreases with further doping when $x > 0.07$. Since the overdoped region is affected by the coexistence of the 10-3-8 and 10-4-8 phases, we could not obtain the overdoped sample of the pure 10-3-8 phase in which superconductivity is fully suppressed. In the whole superconducting region, most samples show a minimum in the normal-state resistivity curve. It should be mentioned that the temperature of resistivity minima T_{min} has an overall trend of shifting to lower temperatures upon Pt doping. The typical temperature of resistivity minimum is about 150–200 K for the underdoped samples, 90–115 K for the optimally doped samples, and 50–70 K for the overdoped samples. Neither an abrupt slope break at T_{min} nor the other anomalies, which can be attributed to a phase transition has ever been observed in the resistivity curves for all the samples, consistent with the previous reports.[18,20] Below T_{min}, the resistivity curves show an upturn, which becomes less pronounced upon Pt doping. Similar phenomena have been reported in 1111 Fe-based superconductors with element substitution within FeAs layers[28–30] and superconducting phosphides, such as $BaRh_2P_2$.[31] This behavior has been explained as an effect of weak localization or spin-flip scattering. However, the upturn is suppressed by Pt doping, which is in contradiction to the prediction of Anderson localization theory,[29] meanwhile, it is hard to accept the Kondo-like scenario since Pt substitution

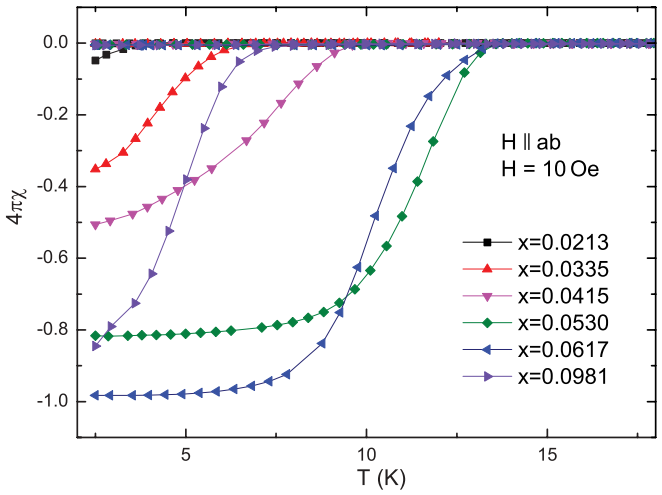

FIG. 3. (Color online) The temperature dependence of in-plane magnetic susceptibility for superconducting $Ca_{10}(Pt_3As_8)((Fe_{1-x}Pt_x)_2As_2)_5$ samples with magnetic fields of 10 Oe.

does not introduce local moments as Co or Ni doping. Up to now, the reason of this upturn remains unclear.

Figure 3 presents the temperature dependence of magnetic susceptibility χ of the superconducting samples measured under zero-field-cooling and field-cooling procedures by applying a magnetic field of 10 Oe along the ab plane at low temperatures. All the samples with $x < 0.02$ show no diamagnetic signal above 2 K (not shown). For the sample with $x = 0.0213$ in which zero resistivity was not observed, the diamagnetism signal can already be observed below the temperature $T_c = 4.3$ K, even though the magnetic shielding fraction is estimated to be less than 5%. Taking the nonuniform Pt distribution in the sample into account, we suggest that the edge of the superconducting region should be at a doping level between $x = 0.020$ and $x = 0.025$. The shielding fraction at 2.5 K exceeds 30% for samples with $x > 0.03$, reaches 80% for samples with $x > 0.05$, and reaches approximately 100% for the optimally doped sample with $x = 0.0617$, indicating bulk superconductivity in these samples. The superconducting transition temperature T_c in the magnetic measurement is consistent with the zero resistivity temperature in the electric measurement. Samples with doping levels of $x = 0.0530$ and $x = 0.0617$ have the maximum transition temperature in the 10-3-8 phase with $T_c = 13.6$ K, which is inconsistent with the result reported by Kakiya *et al.*[20]

In Figs. 4(a)–4(e), we present the resistivity data of two superconducting samples in a low-temperature region under different fields. The samples studied were an underdoped one with $x = 0.0474$ and $T_c = 11.1$ K and an optimally doped sample with $x = 0.0617$ and $T_c = 13.6$ K (the value of T_c was determined by the susceptibility measurements). As there is a pronounced semiconductorlike behavior below T_{min} and preceding the onset of the superconducting transition, a round maximum of resistivity is formed at low temperatures. The drop in resistivity below the temperature of this maximum is not very sharp. The interval between the maximum and the temperature at which resistivity reaches zero is as wide as about 15 K even in the optimally doped sample (see the inset of Fig. 2). As a result, it is rather difficult to determine the onset temperature of superconductivity from the resistivity measurement. We chose three criteria of T_c as 90%, 50%, and 10% of the normal-state resistivity (determined as the local resistivity maxima at low temperatures) and defined three critical fields H_{C2}^{max}, H_{C2}^{mid}, and H_{C2}^{min} following the three criteria, respectively. All the critical fields are shown in Figs. 4(c) and 4(f). For the underdoped sample $x = 0.0474$, the behavior of the critical fields is sensitive to the used criterion. When the magnetic field is applied perpendicular to the ab plane, H_{C2}^{max} shows a negative curvature, whereas, H_{C2}^{min} obviously shows positive curvature, and H_{C2}^{mid} has a nearly linear T dependence. As for the case of $H \parallel ab$, the results are similar, but the curvatures are not so obvious. By using the Werthamer-Helfand-Hohenberg (WHH) formula,[32] the upper critical field at zero temperature can be estimated from the initial slope $(dH_{C2}/dT)_{T=T_c}$. Under the 50% criterion, the value of $H_{C2}(0)$ is about 143.4 T for the configuration of $H \parallel ab$ and about 14.13 T for $H \perp ab$. The anisotropy parameter $\Gamma = H_{C2}^{\parallel}/H_{C2}^{\perp}$ is derived to be about 10, which is much larger than those of $NdFeAsO_{0.82}F_{0.18}$ ($\Gamma \leqslant 6$) (Ref. 33) and doped Ba-122 superconductors [$\Gamma \sim 1.5$-2 for $Ba(Fe_{0.9}Co_{0.1})_2As_2$ (Ref. 34) and $Ba_{0.6}K_{0.4}Fe_2As_2$ (Ref. 35)]. Although the application of the WHH model is questionable since this material was proved to be a multiband system,[36] the results, at least, indicate that the anisotropy of the 10-3-8 phase is probably larger than those in the 1111- and 122-type Fe pnictides. The negative curvature of H_{C2}^{max} is not common in the iron-based superconductors, and it may be affected seriously by the magnetoresistance of the normal state since it is difficult to fix the onset of superconductivity. On the other hand, H_{C2}^{min} could be interpreted as the irreversibility field, and the upward behavior resembles those in $LaFeAsO_{0.89}F_{0.11}$ (Ref. 37) and $Sr_4V_2O_6Fe_2As_2$ (Ref. 12). For the optimally doped sample, an upward curvature was observed in all the critical field curves and was especially distinct for $H \perp ab$. Similar behavior has been reported in cuprates,[38] MgB_2,[39] and Fe-based 1111 superconductors.[33,40] In 1111 Fe pnictides, this upward curvature was usually considered as a result of the two-band effect.[37,40] However, in the 10-3-8 phase, the critical-field curves show an upward bending near T_c, which is more pronounced than most of the other Fe-pnictide superconductors. This anomalous upturn has been theoretically interpreted as an effect of the two-dimensional (2D) nature and is associated with anisotropic Ginzburg-Landau behavior in the dirty limit.[41] Those properties of upper critical fields in the underdoped and optimally doped samples have been confirmed by the measurements on other several pieces of crystals with approximative doping concentrations, and the shape of the curves showed quite weak sample dependence. Additionally, the large interval exists between the resistivity curves under zero field, and $H = 0.5$ T in optimally doped samples might be due to the inhomogeneity of the Pt distribution, which forms small regions with higher T_c and in which the superconductivity is easily suppressed by low magnetic fields. Nonetheless, the data of XRD and susceptibility afford no evidence that supports this assumption.

In order to confirm that there was no magnetic transition existing in the 10-3-8 phase, the normal-state susceptibility measurements were performed. Temperature dependence of

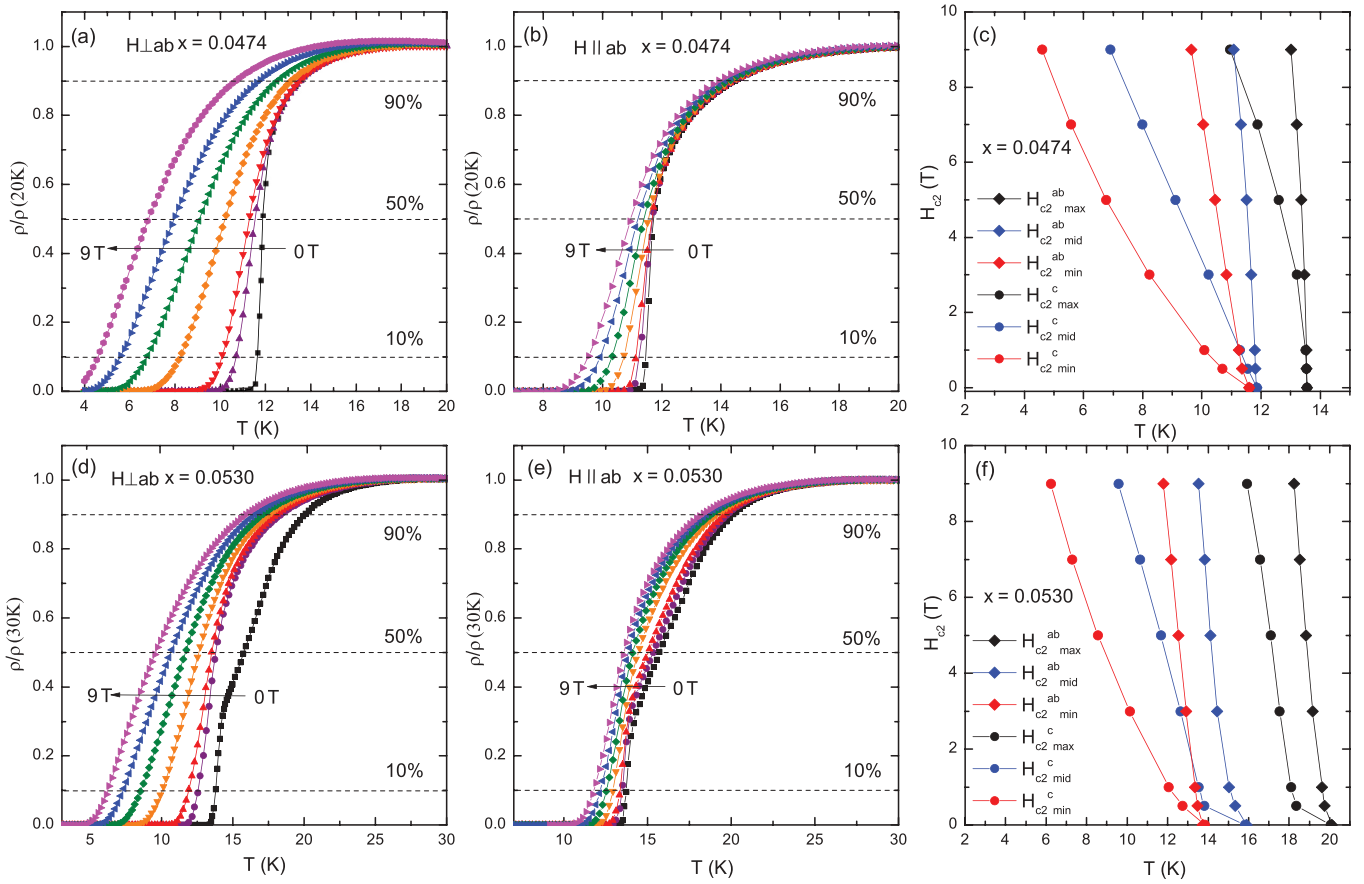

FIG. 4. (Color online) In-plane electrical resistivity in magnetic fields [$H = 0$ T (black), 0.5 T (purple), 1 T (red), 3 T (orange), 5 T (olive), 7 T (blue), and 9 T (magenta), respectively] with (a) and (d) $H \perp ab$ and (b) and (e) $H \parallel ab$ and upper critical fields under different criteria for $Ca_{10}(Pt_3As_8)((Fe_{1-x}Pt_x)_2As_2)_5$ samples with (a)–(c) $x = 0.0474$ and (d)–(f) $x = 0.0530$.

the in-plane susceptibility (measured with the magnetic field lying within the ab plane) for samples with different Pt concentrations in the temperature range from 2 to 300 K under $H = 5$ T are plotted in Fig. 5. For the undoped sample, the susceptibility χ first decreases when cooling from 300 K,

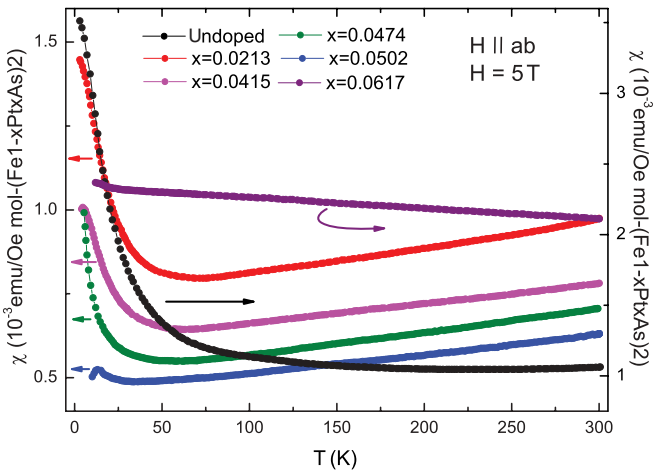

FIG. 5. (Color online) The temperature dependence of the in-plane normal-state magnetic susceptibility for $Ca_{10}(Pt_3As_8)((Fe_{1-x}Pt_x)_2As_2)_5$ single crystals under $H = 5$ T.

and below about 270 K, the slope diminishes gradually and then changes its sign smoothly at about 220–230 K. The temperature dependence of susceptibility is rather weak from 300 to 100 K, and below ~75 K, the susceptibility shows a Curie-like upturn. Again, no magnetic anomalies could be observed in the whole temperature region from 300 to 2 K, which is different from iron-based parent compounds of 1111 and 122 systems. The paramagnetic behavior in the low-temperature region has also been reported in layered non-superconducting Fe-oxypnictides $Sr_3Sc_2O_5Fe_2As_2$ (Ref. 42) and $Sr_4Sc_2O_6Fe_2As_2$.[26] For the underdoped superconducting samples, the in-plane susceptibility exhibits a T-linear behavior above ~70 K, which is similar to those observed at high temperatures in the underdoped $LaO_{1-x}F_xFeAs$ and 122 materials AFe_2As_2 (A = Ca, Sr, Ba).[5,23,43,44] The slope of the T-linear susceptibility decreases slightly upon Pt doping (with 6.63×10^{-7} emu mol^{-1} K^{-1} for $x = 0.0213$, and 5.57×10^{-7} emu mol^{-1} K^{-1} for $x = 0.0502$). The T-linear behavior has been explained as an effect of strong (π,π) SDW fluctuations, and the slope is determined by the square of the SDW amplitude with nesting momentum $\mathbf{Q} = (\pi,\pi)$.[45] Since the slope of T-linear susceptibility in the 10-3-8 phase lies between the value of the slope of Ni-doped LaFeAsO (Ref. 29) and Co-doped $BaFe_2As_2$,[5] we can conclude that, even though there is no AFM ordering in the 10-3-8 phase,

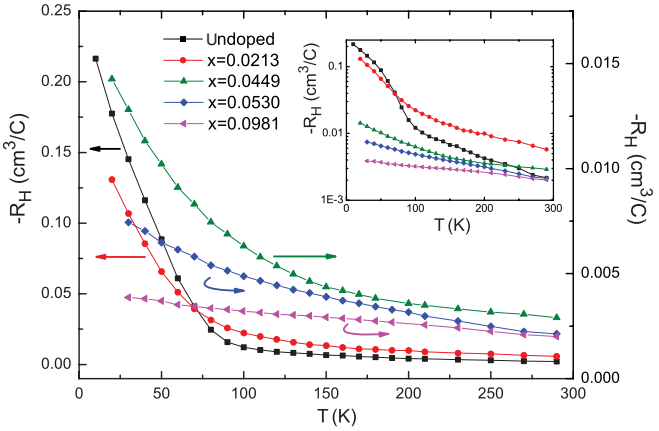

FIG. 6. (Color online) The temperature dependence of Hall coefficient R_H for $Ca_{10}(Pt_3As_8)((Fe_{1-x}Pt_x)_2As_2)_5$ samples. The inset shows the same data on a logarithmic scale.

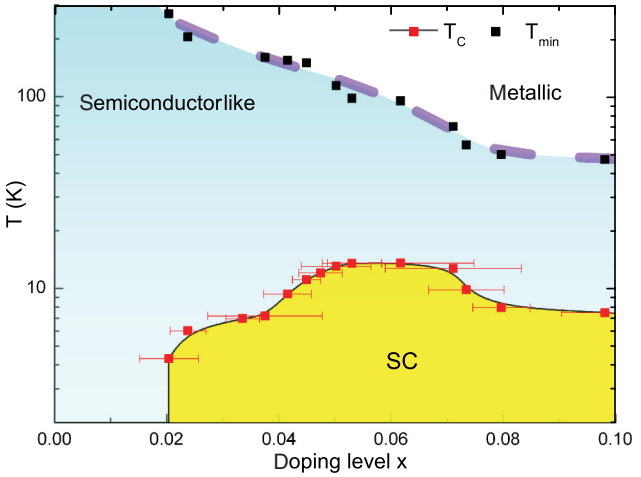

FIG. 7. (Color online) Electronic phase diagram for $Ca_{10}(Pt_3As_8)((Fe_{1-x}Pt_x)_2As_2)_5$. T_{min} indicates the resistivity minimum temperature. T_c was determined by susceptibility measurement.

strong AFM spin fluctuations still exist in this system and may play an important role in inducing superconductivity. At low temperatures, the susceptibility of all the underdoped samples shows an obvious upturn, which has also been reported in many other Fe-pnictide superconductors.[28,29,46] We attempted to fit the low-temperature susceptibility of both undoped and underdoped samples using the Curie-Weiss formula. For underdoped samples, we obtained small effective moments ($\sim 0.1\mu_B$ per Fe site), which shows considerable sample dependence, whereas, for the undoped samples, the Curie constant is 1 order of magnitude larger. Thus, we believe that the Curie-Weiss-type behavior in the underdoped samples is likely to be extrinsic and could be ascribed to impurities and defects as is the case in 1111 materials, whereas, in the semiconducting undoped compound, the paramagnetic behavior at low temperatures might be intrinsic as in nonsuperconducting 32 522 and 42 622 systems. For the optimally doped and slightly overdoped samples, the T-linear behavior is broken, and χ is nearly temperature independent down to the onset of superconductivity; both the behavior and the magnitude are similar to those in optimally doped 122-type Fe-pnictide superconductors.[21,47]

Figure 6 shows the temperature-dependent Hall coefficients for $Ca_{10}(Pt_3As_8)((Fe_{1-x}Pt_x)_2As_2)_5$ crystals with different Pt contents. We checked the linearity of the Hall voltage in H up to 5 T. For all of the samples, the Hall coefficient R_H remains negative in the whole temperature regime from T_c to 300 K, which indicates that electron-type charge carriers dominate the conduction in all the samples. The absolute value of R_H of the undoped sample is about twice as large as that of SmFeAsO (Ref. 48) at low temperatures, but there is no anomaly in the slope of the R_H, which could be related to magnetic transition. Nonetheless, the Hall coefficient of the undoped sample as well as the underdoped samples shows a strong temperature dependence at low temperatures, which suggests either a strong multiband effect or a spin-related scattering effect.[42] With increasing the Pt-doping level, this temperature dependence becomes moderate and almost vanishes for the overdoped samples. The Hall concentration $n_H = 1/(eR_H)$, which represents carrier concentration in the single-band model, however, does not follow a monotonic doping dependence at high temperatures. As shown in the inset of Fig. 6, underdoped samples with $x = 0.0213$ and $x = 0.0449$ have larger R_H, that is, smaller Hall concentration than the undoped sample at room temperature. With enhancing Pt content, the Hall concentration first decreases in the underdoped region and then increases upon further doping. The turning point depends on temperature. All of these behaviors, except for the absence of SDW transition, are similar to those in $Ba(Fe_{1-x}Co_x)_2As_2$,[49,50] which could be explained under a multiband model as the competing effect of carrier doping and hole mobility decreasing in the underdoped region.

Based on the data of transport and magnetic measurements shown above, an electronic phase diagram for the $Ca_{10}(Pt_3As_8)((Fe_{1-x}Pt_x)_2As_2)_5$ system was summarized in Fig. 7. The unsubstituted compound $Ca_{10}(Pt_3As_8)(Fe_2As_2)_5$ is a heavily doped semiconductor without magnetic ordering, different from the parent compounds of 1111 and 122 Fe-pnictide superconductors, which are antiferromagnetic bad metals. The Pt substitution on the Fe site dopes electrons to the Fe_2As_2 layer as proved by the Hall coefficient measurements. About 2% Pt doping begins to introduce superconductivity, and T_c reaches its maximum of $T_c^{max} = 13.6$ K in the doping range of $0.050 < x < 0.065$. Further Pt doping makes T_c decrease slowly. With the doping level up to $x \sim 0.1$, superconducting transition can still be observed at about 7.4 K, and with further doping, the single 10-3-8 phase cannot be obtained. Therefore, the superconducting phase region is extremely asymmetric as in the Pt-doped Ba-122 system.[51] The normal state is divided by the line of T_{min} into semiconducting and metallic regions, which is similar to Co-doped and Ni-doped 1111 systems.[28,29] The most extraordinary aspect of the phase diagram is the absence of an AFM region, which exists in the underdoped side of the electronic phase diagram for all of the 1111 and 122 Fe-pnictide materials.[7,52] In the former phase diagram established by Cho *et al.*,[53] the magnetic and superconducting phases are clearly separated. In this paper, we performed resistivity, susceptibility, and Hall coefficient measurements, and all of the data indicated the fact that there was actually

neither SDW nor other types of magnetic order existing in the phase diagram of the 10-3-8 system.

As mentioned above, static magnetic order is also absent in LiFeAs and perov-FeAs compounds. In the latter case, due to the large thickness of the perovskite-type blocking layer, the distance between the two nearest FeP layers is more than ~13 Å,[54] which is much larger than other types of layered iron pnictides. It is believed that the much stronger two-dimensional character compared to other Fe-pnictide superconductors, which causes relatively weak magnetic coupling between FeAs layers, is destructive to the antiferromagnetic correlation between the moments of Fe ions in the neighboring FeAs layers and then prevents the system from forming a long-range magnetic order.[26,42,54–56] In the 10-3-8 phase, the distance between the two neighboring Fe_2As_2 layers is about 10.2 Å, which is smaller than that in perov-FeAs materials but is still larger than that in the 1111 materials ($d \sim 8.4$–8.9 Å) and 122 materials ($d \sim 5.8$–6.6 Å). The highly anisotropic 2D nature of $Ca_{10}(Pt_3As_8)((Fe_{1-x}Pt_x)_2As_2)_5$ is already indicated by our anisotropy parameter studies of the upper critical field and the similar result by Ni *et al.*[18] Thus, it is possible that the weak interlayer coupling suppresses the antiferromagnetic order in the 10-3-8 phase as in perov-FeAs materials. However, the linear T dependence of susceptibility at high temperatures indicates that antiferromagnetic spin fluctuation still exists in the 10-3-8 phase, although magnetic ordering is suppressed. Strong antiferromagnetic spin fluctuations have been observed in LiFeAs (Ref. 57) and $(Ca_4Al_2O_{6-y})(Fe_2As_2)$,[54] both of which have no magnetic order close to or coexisting with superconductivity. Therefore, it is reasonable to conclude that there is also a crucial relationship between AFM spin fluctuations and superconductivity in these materials, including the 10-3-8 phase, as in the other existing Fe-pnictide superconductors, which exhibit magnetic order in their parent compounds.

IV. CONCLUSION

To summarize, high-quality $Ca_{10}(Pt_3As_8)((Fe_{1-x}Pt_x)_2As_2)_5$ single crystals with doping level $0 \leqslant x < 0.1$ were successfully grown by the self-flux method. A systematic study of the transport and magnetic properties of the single-crystal samples was performed, and an electronic phase diagram was established. The undoped sample is a semiconductor without any type of magnetic order. Pt substitution on the Fe site dopes electrons into the Fe_2As_2 layers and introduces metallic resistivity behavior and superconductivity. In the phase diagram, there is no AFM region, which is a notable difference from the phase diagram of 1111- and 122-type Fe-pnictide materials. We argued that the absence of long-range AFM order is due to the strong 2D character of this system, which is revealed by the relatively large anisotropy parameter Γ. The extremely anisotropic nature weakens the interlayer coupling as in the perovskite-type layered Fe-based compounds. Apart from that, the properties of the superconducting samples are similar to other electron-doped Fe-pnictide superconductors, indicating that the properties of this system are dominated by Fe_2As_2 layers. This is inconsistent with previous results that the Pt_3As_8 layers couple only weakly with the Fe_2As_2 layers, and the contribution of density of states at the Fermi level from Pt is rather small.[19,36] For underdoped samples, the magnetic susceptibility shows T-linear dependence in a wide temperature range, indicating strong magnetic fluctuation in this system. This result suggests that the mechanism of superconductivity of $Ca_{10}(Pt_3As_8)((Fe_{1-x}Pt_x)_2As_2)_5$ is likely to be similar to that in other iron-based superconductors. Being a special member of the layered Fe-pnictide superconductor family with no magnetic order and showing variation in the ground state from the paramagnetic semiconductor to the superconductor controlled by electron doping, the 10-3-8 phase is a good candidate for studying the interplay between magnetism and superconductivity in Fe-pnictide superconductors. Further research on the magnetic fluctuations in this system may help to understand the mechanism and nature of high-temperature superconductivity.

ACKNOWLEDGMENTS

This work was supported by the National Natural Science Foundation of China (Grants No. 11190020 and No. 51021091), the National Basic Research Program of China (973 Program, Grants No. 2012CB922002 and No. 2011CB00101), and the Chinese Academy of Sciences.

*Corresponding author: chenxh@ustc.edu.cn

[1] H. Chen, Y. Ren, Y. Qiu, W. Bao, R. H. Liu, G. Wu, T. Wu, Y. L. Xie, X. F. Wang, Q. Huang, and X. H. Chen, Europhys. Lett. **85**, 17006 (2009).

[2] H. Luetkens, H.-H. Klauss, M. Kraken, F. J. Litterst, T. Dellmann, R. Klingeler, C. Hess, R. Khasanov, A. Amato, C. Baines, M. Kosmala, O. J. Schumann, M. Braden, J. Hamann-Borrero, N. Leps, A. Kondrat, G. Behr, J. Werner, and B. Büchner, Nature Mater. **8**, 305 (2009).

[3] J. Zhao, Q. Huang, C. de la Cruz, S. L. Li, J. W. Lynn, Y. Chen, M. A. Green, G. F. Chen, G. Li, Z. Li, J. L. Luo, N. L. Wang, and P. C. Dai, Nature Mater. **7**, 953 (2008).

[4] A. J. Drew, C. Niedermayer, P. J. Baker, F. L. Pratt, S. J. Blundell, T. Lancaster, R. H. Liu, G. Wu, X. H. Chen, I. Watanabe, V. K. Malik, A. Dubroka, M. Rössle, K. W. Kim, C. Baines, and C. Bernhard, Nature Mater. **8**, 310 (2009).

[5] X. F. Wang, T. Wu, G. Wu, R. H. Liu, H. Chen, Y. L. Xie, and X. H. Chen, New J. Phys. **11**, 045003 (2009).

[6] F. Wang and D.-H. Lee, Science **332**, 200 (2011).

[7] M. D. Lumsden and A. D. Christianson, J. Phys.: Condens. Matter **22**, 203203 (2010).

[8] I. I. Mazin, D. J. Singh, M. D. Johannes, and M. H. Du, Phys. Rev. Lett. **101**, 057003 (2008).

[9] A. V. Chubukov, D. V. Efremov, and I. Eremin, Phys. Rev. B **78**, 134512 (2008).

[10] V. Cvetkovic and Z. Tesanovic, Europhys. Lett. **85**, 37002 (2009).

[11] S. V. Borisenko, V. B. Zabolotnyy, D. V. Evtushinsky, T. K. Kim, I. V. Morozov, A. N. Yaresko, A. A. Kordyuk, G. Behr, A. Vasiliev, R. Follath, and B. Büchner, Phys. Rev. Lett. **105**, 067002 (2010).

[12] X. Zhu, F. Han, G. Mu, P. Cheng, B. Shen, B. Zeng, and H.-H. Wen, Phys. Rev. B **79**, 220512 (2009).

[13]H. Ogino, Y. Shimizu, N. Kawaguchi, K. Kishio, J.-i. Shimoyama, T. Tohei, and Y. Ikuhara, Supercond. Sci. Technol. **24**, 085020 (2011).
[14]H. Ogino, K. Machida, A. Yamamoto, K. Kishio, J.-i. Shimoyama, T. Tohei, and Y. Ikuhara, Supercond. Sci. Technol. **23**, 115005 (2010).
[15]P. M. Shirage, K. Kihou, C.-H. Lee, H. Kito, H. Eisaki, and A. Iyo, J. Am. Chem. Soc. **133**, 9630 (2011).
[16]P. M. Shirage, K. Kihou, C.-H. Lee, H. Kito, H. Eisaki, and A. Iyo, Appl. Phys. Lett. **97**, 172506 (2010).
[17]H. Ogino, Y. Shimizu, K. Ushiyama, N. Kawaguchi, K. Kishio, and J. Shimoyama, J. Appl. Phys. Exp. **3**, 063103 (2010).
[18]N. Ni, J. M. Allred, B. C. Chan, and R. J. Cava, Proc. Natl. Acad. Sci. USA **108**, 1019 (2011).
[19]C. Löhnert, T. Stürzer, M. Tegel, R. Frankovsky, G. Friederichs, and D. Johrendt, Angew. Chem. Int. Ed. **50**, 9195 (2011).
[20]S. Kakiya, K. Kudo, Y. Nishikubo, K. Oku, E. Nishibori, H. Sawa, T. Yamamoto, T. Nozaka, and M. Nohara, J. Phys. Soc. Jpn. **80**, 093704 (2011).
[21]S. R. Saha, T. Drye, K. Kirshenbaum, N. P. Butch, P. Y. Zavalij, and J. Paglione, J. Phys.: Condens. Matter **22**, 072204 (2010).
[22]K. Kirshenbaum, S. R. Saha, T. Drye, and J. Paglione, Phys. Rev. B **82**, 144518 (2010).
[23]X. F. Wang, T. Wu, G. Wu, H. Chen, Y. L. Xie, J. J. Ying, Y. J. Yan, R. H. Liu, and X. H. Chen, Phys. Rev. Lett. **102**, 117005 (2009).
[24]M. A. McGuire, A. D. Christianson, A. S. Sefat, B. C. Sales, M. D. Lumsden, R. Jin, E. A. Payzant, D. Mandrus, Y. Luan, V. Keppens, V. Varadarajan, J. W. Brill, R. P. Hermann, M. T. Sougrati, F. Grandjean, and G. J. Long, Phys. Rev. B **78**, 094517 (2008).
[25]Y. Kamihara, T. Watanabe, M. Hirano, and H. Hosono, J. Am. Chem. Soc. **130**, 3296 (2008).
[26]Y. L. Xie, R. H. Liu, T. Wu, G. Wu, Y. A. Song, D. Tan, X. F. Wang, H. Chen, J. J. Ying, Y. J. Yan, Q. J. Li, and X. H. Chen, Europhys. Lett. **86**, 57007 (2009).
[27]Y. J. Yan, M. Zhang, A. F. Wang, J. J. Ying, Z. Y. Li, W. Qin, X. G. Luo, J. Q. Li, J. Hu, and X. H. Chen, Sci. Rep. **1**, 212 (2011).
[28]C. Wang, Y. K. Li, Z. W. Zhu, S. Jiang, X. Lin, Y. K. Luo, S. Chi, L. J. Li, Z. Ren, M. He, H. Chen, Y. T. Wang, Q. Tao, G. H. Cao, and Z. A. Xu, Phys. Rev. B **79**, 054521 (2009).
[29]G. Cao, S. Jiang, X. Lin, C. Wang, Y. Li, Z. Ren, Q. Tao, C. Feng, J. Dai, Z. Xu, and F.-C. Zhang, Phys. Rev. B **79**, 174505 (2009).
[30]S. J. Singh, J. Prakash, S. Patnaik, and A. K. Ganguli, Physica C **470**, 1928 (2010).
[31]N. Berry, C. Capan, G. Seyfarth, A. D. Bianchi, J. Ziller, and Z. Fisk, Phys. Rev. B **79**, 180502 (2009).
[32]N. R. Werthamer, E. Helfand, and P. C. Hohenberg, Phys. Rev. **147**, 295 (1966).
[33]Y. Jia, P. Cheng, L. Fang, H. Luo, H. Yang, C. Ren, L. Shan, C. Gu, and H.-H. Wen, Appl. Phys. Lett. **93**, 032503 (2008).
[34]A. Yamamoto, J. Jaroszynski, C. Tarantini, L. Balicas, J. Jiang, A. Gurevich, D. C. Larbalestier, R. Jin, A. S. Sefat, M. A. McGuire, B. C. Sales, D. K. Christen, and D. Mandrus, Appl. Phys. Lett. **94**, 062511 (2009).
[35]Z.-S. Wang, H.-Q. Luo, C. Ren, and H.-H. Wen, Phys. Rev. B **78**, 140501 (2008).
[36]M. Neupane, C. Liu, S.-Y. Xu, Y. J. Wang, N. Ni, J. M. Allred, L. A. Wray, N. Alidoust, H. Lin, R. S. Markiewicz, A. Bansil, R. J. Cava, and M. Z. Hasan, Phys. Rev. B **85**, 094510 (2012).
[37]F. Hunte, J. Jaroszynski, A. Gurevich, D. C. Larbalestier, R. Jin, A. S. Sefat, M. A. McGuire, B. C. Sales, D. K. Christen, and D. Mandrus, Nature (London) **453**, 903 (2008).
[38]M. S. Osofsky, R. J. Soulen Jr., S. A. Wolf, J. M. Broto, H. Rakoto, J. C. Ousset, G. Coffe, S. Askenazy, P. Pari, I. Bozovic, J. N. Eckstein, and G. F. Virshup, Phys. Rev. Lett. **71**, 2315 (1993).
[39]K.-H. Müller, G. Fuchs, A. Handstein, K. Nenkov, V. N. Narozhnyi, and D. Eckert, J. Alloys Compd. **322**, L10 (2001).
[40]J. Jaroszynski, F. Hunte, L. Balicas, Y.-j. Jo, I. Raicevic, A. Gurevich, D. C. Larbalestier, F. F. Balakirev, L. Fang, P. Cheng, Y. Jia, and H. H. Wen, Phys. Rev. B **78**, 174523 (2008).
[41]T. Schneider, IBM Res. Dev. **33**, 351 (1989).
[42]X. Zhu, F. Han, G. Mu, B. Zeng, P. Cheng, B. Shen, and H.-H. Wen, Phys. Rev. B **79**, 024516 (2009).
[43]G. Wu, H. Chen, T. Wu, Y. L. Xie, Y. J. Yan, R. H. Liu, X. F. Wang, J. J. Ying, and X. H. Chen, J. Phys.: Condens. Matter **20**, 422201 (2008).
[44]R. Klingeler, N. Leps, I. Hellmann, A. Popa, U. Stockert, C. Hess, V. Kataev, H.-J. Grafe, F. Hammerath, G. Lang, S. Wurmehl, G. Behr, L. Harnagea, S. Singh, and B. Büchner, Phys. Rev. B **81**, 024506 (2010).
[45]M. M. Korshunov, I. Eremin, D. V. Efremov, D. L. Maslov, and A. V. Chubukov, Phys. Rev. Lett. **102**, 236403 (2009).
[46]R. E. Baumbach, J. J. Hamlin, L. Shu, D. A. Zocco, N. M. Crisosto, and M. B. Maple, New J. Phys. **11**, 025018 (2009).
[47]N. Kumar, R. Nagalakshmi, R. Kulkarni, P. L. Paulose, A. K. Nigam, S. K. Dhar, and A. Thamizhavel, Phys. Rev. B **79**, 012504 (2009).
[48]R. H. Liu, G. Wu, T. Wu, D. F. Fang, H. Chen, S. Y. Li, K. Liu, Y. L. Xie, X. F. Wang, R. L. Yang, L. Ding, C. He, D. L. Feng, and X. H. Chen, Phys. Rev. Lett. **101**, 087001 (2008).
[49]L. Fang, H. Luo, P. Cheng, Z. Wang, Y. Jia, G. Mu, B. Shen, I. I. Mazin, L. Shan, C. Ren, and H.-H. Wen, Phys. Rev. B **80**, 140508 (2009).
[50]F. Rullier-Albenque, D. Colson, A. Forget, and H. Alloul, Phys. Rev. Lett. **103**, 057001 (2009).
[51]X. Zhu, F. Han, G. Mu, P. Cheng, J. Tang, J. Ju, K. Tanigaki, and H.-H. Wen, Phys. Rev. B **81**, 104525 (2010).
[52]P. C. Canfield, S. L. Budko, N. Ni, J. Q. Yan, and A. Kracher, Phys. Rev. B **80**, 060501 (2009).
[53]K. Cho, M. A. Tanatar, H. Kim, W. E. Straszheim, N. Ni, R. J. Cava, and R. Prozorov, Phys. Rev. B **85**, 020504(R) (2012).
[54]H. Kinouchi, H. Mukuda, M. Yashima, Y. Kitaoka, P. M. Shirage, H. Eisaki, and A. Iyo, Phys. Rev. Lett. **107**, 047002 (2011).
[55]A. S. Sefat, D. J. Singh, V. Ovidiu Garlea, Y. L. Zuev, M. A. McGuire, and B. C. Sales, Physica C **471**, 143 (2011).
[56]J. Munevar, D. R. Sánchez, M. Alzamora, E. Baggio-Saitovitch, J. P. Carlo, T. Goko, A. A. Aczel, T. J. Williams, G. M. Luke, H.-H. Wen, X. Zhu, F. Han, and Y. J. Uemura, Phys. Rev. B **84**, 024527 (2011).
[57]A. E. Taylor, M. J. Pitcher, R. A. Ewings, T. G. Perring, S. J. Clarke, and A. T. Boothroyd, Phys. Rev. B **83**, 220514 (2011).